Voltammetry as Virtual Potentiometric Sensor in Modelling of a Metal/Ligand System and Refinement of Stability Constants

Part 5

Complexation Studies of Hydrolysis-Prone Lead(II) with Glycine and Sarcosine by Sampled-Direct-Current Polarography Involving Virtual Potential

by **Ignacy Cukrowski***, **Philemon Magampa**, and **Tumaini Samuel Mkwizu**

Department of Chemistry, University of Pretoria, Pretoria, 0002 South Africa
(phone: +27 12 420-2512; fax: +27 12 362-5297; e-mail: ignacy.cukrowski@up.ac.za)

The concept of virtual potential (employed here in modelling operations), a unique experimental setup designed and built in our laboratories, and new regression equations derived for nonlinear fitting of quasi-reversible direct-current polarograms were combined with the existing rigorous treatment and refinement of polarographic data to establish reliable metal/ligand models and accurate stability constants for the lead(II)/glycine/OH^- and lead(II)/sarcosine/OH^- systems (sarcosine = *N*-methylglycine). In the case of glycine, the complexes [M(HL)], [ML], [ML_2], and [ML_3] were identified, and their stability constants (as log β) were established to be 10.51 ± 0.06, 4.58 ± 0.02, 7.19 ± 0.10, and 9.27 ± 0.02, respectively, the complex [ML_3] being reported here for the first time (*Table 2*). The system with sarcosine involving [M(HL)], [ML], [ML_2], [ML_3], and [$ML_2(OH)_2$], with the stability constants (as log β) 11.01 ± 0.04, 4.18 ± 0.03, 7.23 ± 0.03, 9.1 ± 0.3, and 15.97 ± 0.07, respectively, is reported for the first time (*Table 3*). The log K_1 value for Pb^{II} with sarcosine is a fraction of a log unit smaller when compared with the Pb^{II} complex with glycine, in agreement with the literature data for Cu^{II}, Ni^{II}, and Zn^{II} showing the same trend for these two ligands. The proposed nonlinear curve-fitting operations expand the applicability of polarography to study reliably and conveniently quasi-reversible, on the polarographic time scale, metal/ligand systems (systems with involved heterogeneous kinetics).

Introduction. – The quality of experimental research work depends on several factors, among them the accuracy and reproducibility of measurements performed, the number of data points collected, and the rigorous application of existing theories and methodologies. In the case of the study of metal complexes, potentiometry and spectroscopy can be regarded as nondisturbing homogeneous-equilibrium analytical techniques. The theoretical treatment of data collected is exactly the same in case of very fast, very slow, or intermediate homogeneous equilibria; the only requirement is that the measurement must be taken when all species involved are at thermodynamic equilibrium. The above conditions made the related theories reasonably simple. As any analytical technique, however, potentiometry and spectroscopy have many limitations [1], and hence other analytical techniques are needed, not only to study a metal/ligand system when potentiometry or spectroscopy fail, but also to verify models and stability constants obtained from the two techniques.

An obvious advantage of using voltammetry is the ability of working at a low total metal-ion concentration ($[M_T]$) and a large ratio $[L_T]/[M_T]$ of the total ligand ($[L_T]$) and metal-ion concentration [2–6]; voltammetry can operate in a much larger analytical domain [1] and at much lower pH values [6][7] when compared with, *e.g.*, potentiometry. Unfortunately, being an interfacial and homogeneous-equilibrium-disturbing (within a *Nernst* diffusion layer) analytical technique, voltammetric theories must take into account heterogeneous kinetics (an electron transfer between an electrode surface and an adjacent solution layer) and homogeneous kinetics (equilibria among all species in a solution). As a result, there is not a single theory describing voltammetric data in the field of metal/ligand equilibrium studies [5][8–13].

Recently developed theory allows to study by polarography metal/ligand systems that might be regarded as labile [14–16], inert [17][18], or intermediate [19] on the polarographic time scale. It requires, however, that recorded polarograms can be regarded as polarographically reversible and are the result of a reduction of only fully labile species. The power and versatility of polarography in the study of metal complexes was recently extended by introducing a new concept of virtual potential [1][6][7][20].

The analysis of literature data [21][22] reveals that the data for lead(II) complexes with the ligand glycine are characterized by a quite large uncertainty. The Analytical Chemistry Division of IUPAC has commissioned a critical survey on stability constants of glycine complexes; almost 300 publications have been evaluated [22]. This survey reveals a rich contribution from several analytical techniques when the Pb^{II}/glycine system is concerned. Unfortunately, due to the spread in the reported stabilities, there is no solid recommendation for stability constants for the Pb^{II}/glycine/OH^- model. Even worse applies to the Pb^{II}/sarcosine system (sarcosine = *N*-methylglycine) as, to the best of our knowledge, no data were reported to date for that system.

The aim of this work is to establish reliable metal/ligand models and as accurate as possible stability constants for the complexes formed for the Pb^{II}/glycine/OH^- and Pb^{II}/sarcosine/OH^- systems. Moreover, the applicability of virtual potential in modelling operations is explored. A fully automated experimental setup is designed and built; this PC-controlled system allows the collection of a large number of experimental data necessary for the refinement of data obtained from a multicomponent metal/ligand system. Also, new nonlinear curve-fitting equations are reported, which are derived from a previously reported logarithmic analysis of polarograms and allow to correct for the departure from electrochemical reversibility. All the above was aimed at obtaining stability constants with an uncertainty smaller than ± 0.1 log units, a requirement difficult to meet by any experimental technique, particularly by polarography.

Theory and Treatment of Data. – *Polarography.* The refinement operations and modelling of direct-current (DC) polarographic data were performed by the method of speciation reported previously [14–19]. This method requires that *i*) the processes observed are electrochemically reversible on the polarographic timescale employed (heterogeneous kinetics, *i.e.*, electron transfer, must be fast), and *ii*) the $[L_T]/[M_T]$ ratio is 30 or larger, except for fully nonlabile metal/ligand systems. The methodology adopted for the analysis of the metal/ligand systems studied in this work by sampled

direct-current polarography (DCP) employed a fixed $[L_T]/[M_T]$ ratio and varied pH as expressed by *Eqn. 1* [20].

$$\left(E_{1/2}(\mathrm{M}) - \left(E_{1/2}(\mathrm{comp})\right)_{\mathrm{pH}(i)}\right) - \frac{RT}{nF}\ln\left(\frac{I(\mathrm{comp})}{I(\mathrm{M})}\right)_{\mathrm{pH}(i)} = \frac{RT}{nF}\ln\left(\frac{[\mathrm{M_T}]}{[\mathrm{M}]}\right)_{\mathrm{pH}(i)} \quad (1)$$

The plot of the left-hand side of *Eqn. 1 vs.* pH generates the experimental complex-formation curve (ECFC). The ECFC is used as the experimental objective function that has to be reproduced by a theoretical function, the computed complex-formation curve (CCFC). The refinement of stability constants is achieved by the computation of the free-metal-ion concentration [M] from mass-balance equations written for the assumed metal/ligand/OH^- model. The computed [M] is then used by the right-hand side of *Eqn. 1*. During the iterative operation, the values of refined stability constants are varied. The refinement operation is completed when the CCFC fits best the experimental objective function, *i.e.*, the ECFC, the goodness-of-fit being judged by the overall fit *OF* (see *Eqn. 2*).

$$OF = \sqrt{\frac{\sum(\mathrm{ECFC} - \mathrm{CCFC})^2_{\mathrm{pH}(i)}}{n-1}} \quad [\mathrm{m}V] \quad (2)$$

The total metal-ion and ligand concentrations, $[M_T]$ and $[L_T]$, are known at any stage of the experiment; appropriate mass-balance equations can be written as *Eqns. 3* and *4*, where β_n^{H} and $\beta_{\mathrm{M}_p\mathrm{L}_q\mathrm{OH}_r}$ stand for the overall protonation and stability constants, respectively, and [M], [L], [H], and [OH] stand for the free-metal-ion, free-ligand, proton, and hydroxide ion concentrations, respectively. In the case of the formation of complexes involving protonated forms of the ligand, *e.g.*, $M(HL)^1$), the term $[M]^p[L]^q[OH]^r$ would be exchanged by $[M]^p[L]^q[H]^r$. It is important to note that, due to a large excess of a ligand, a mass-balance equation for the total proton concentration is not solved when voltammetry is used to study metal complexes. This is the fundamental difference between the polarographic and potentiometric theories and mathematical procedures employed in the field. The free-proton concentration is obtained from a direct measurement performed with a solution sample by a calibrated glass electrode.

$$[\mathrm{M_T}] = [\mathrm{M}] + \sum_{p=1}\sum_{q=1}\sum_{r=0} p\beta_{\mathrm{M}_p\mathrm{L}_q\mathrm{OH}_r}[\mathrm{M}]^p[\mathrm{L}]^q[\mathrm{OH}]^r + \sum_{x=1}\sum_{y=1} x\beta_{\mathrm{M}_x\mathrm{OH}_y}[\mathrm{M}]^x[\mathrm{OH}]^y \quad (3)$$

$$[\mathrm{L_T}] = [\mathrm{L}] + \sum_{p=1}\sum_{q=1}\sum_{r=0} q\beta_{\mathrm{M}_p\mathrm{L}_q\mathrm{OH}_r}[\mathrm{M}]^p[\mathrm{L}]^q[\mathrm{OH}]^r + [\mathrm{L}]\sum_{n=1}\beta_n^{\mathrm{H}}[\mathrm{H}]^n \quad (4)$$

For the final Pb^{II}/glycine/OH^- model reported in this work, *Eqns. 3* and *4* would become *Eqns. 5* and *6*, where K_n^{H} stands for the stepwise-protonation constants of the ligand glycine. The stepwise-protonation constants [21] of the ligand glycine and the hydrolysis constants for Pb^{II} [21] were kept fixed during the refinement operations,

---

[1]) For convenience, the IUPAC-recommended brackets enclosing formulas of complexes are omitted.

and $\beta_{M(HL)}$, β_{ML}, β_{ML_2}, and β_{ML_3} were refined simultaneously[1]). The refinement procedure employed in this work followed the following steps. One starts with initial estimates for the values of the stability constants β_{ML}, β_{ML_2}, and β_{ML_3}, *etc.*; the initial estimates can easily be determined to a fraction of a log unit by using a methodology reported recently [1]. The difference between experimentally known $[M_T]_{pH(i)}$ and computed $[M_T]_{calc}$ values at pH(i) is minimized for a given set of stability constants. This results in a set of computed concentrations of $[M]_{pH(i)}$ and $[L]_{pH(i)}$. The free-metal-ion concentration obtained at each pH(i) value is then used in the right-hand side of *Eqn. 1*. The value generated by the right-hand side of *Eqn. 1* is compared with the left-hand side of *Eqn. 1*, and the function *OF* is computed, which means fitting of the CCFC into the objective function, *i.e.*, the ECFC. The variation in *OF* determines the change in the refined values of the stability constants in such a way that the computed free-metal-ion concentration from *Eqns. 5* and *6* will reproduce best the objective function ECFC for all experimental points collected. The optimization of a given model and refinement of stability constants were carried out with the dedicated computer software 3D–CFC [23].

$$\begin{aligned}[M_T]_{calc} = {} & [M] + \beta_{M(HL)}[M][L][H] + \beta_{ML}[M][L] + \beta_{ML_2}[M][L]^2 + \beta_{ML_3}[M][L]^3 \\ & + \beta_{M(OH)}[M][OH] + \beta_{M(OH)_2}[M][OH]^2 + \beta_{M(OH)_3}[M][OH]^3 \\ & + 2\beta_{M_2(OH)}[M]^2[OH] + 3\beta_{M_3(OH)_4}[M]^3[OH]^4 + 4\beta_{M_4(OH)_4}[M]^4[OH]^4 \\ & + 6\beta_{M_6(OH)_8}[M]^6[OH]^8 \end{aligned} \tag{5}$$

$$\begin{aligned}[L_T]_{calc} = {} & [L] + K_1^H[H][L] + K_1^H K_2^H[H]^2[L] + \beta_{M(HL)}[M][L][H] + \beta_{ML}[M][L] \\ & + 2\beta_{ML_2}[M][L]^2 + 3\beta_{ML_3}[M][L]^3 \end{aligned} \tag{6}$$

Virtual Potentiometry (VP). A recently developed theory and a concept of virtual potentiometry (VP) [1][6][7][20] was used for further modelling of polarographic data. The proposed methodology involves conversion of polarographic data ($I(comp)_{pH(i)}$, $I(M)_{pH(i)}$, and $(E_{1/2}(comp))_{pH(i)}$) into virtual thermodynamic potentials, $E_{1/2}(virt)_{pH(i)}$, calculated from each recorded polarogram at the ith pH value. The virtual potentials are calculated according to *Eqn. 7*. The observed potential of the recorded polarographic signal is equal to the virtual potential only if the intensity of the signal remains unchanged throughout an experiment, *i.e.*, $I(comp) = I(M)$. The larger the decrease in the recorded polarographic signal is, the more significant the difference between the experimental and virtual potential becomes, with the virtual potential being more negative than the observed one. It appears that the virtual potential $E_{1/2}$(virt) rather than $E_{1/2}(comp)$ must be used in modelling of metal/ligand/OH^- systems. This will be illustrated in the discussion of results below when analysis of slopes, such as $E_{1/2}$ *vs.* pH or $E_{1/2}$ *vs.* log [L], is performed.

$$\left(E_{1/2}(comp)\right)_{pH(i)} + \frac{RT}{nF}\ln\left(\frac{I(comp)}{I(M)}\right)_{pH(i)} = E_{1/2}(virt)_{pH(i)} \tag{7}$$

Analysis of Polarograms. Recorded polarographic curves have to be analyzed to establish the degree of electrochemical reversibility and its change throughout the experiment. If there is a variation in the electrochemical reversibility and *Eqn. 1* is employed, the reversible half-wave potential ($E^{r}_{1/2}$) and the limiting diffusion-current (I_d) values from the recorded polarograms at various pH values must be estimated as accurately as possible.

A simple nonlinear curve-fitting method (*Eqn. 8*) for the analysis of DC polarograms for purposes of evaluating electrochemical reversibility has been proposed recently [1][6]. *Eqn. 8* is essentially that describing the current-potential relationship of a reversible DC polarogram with a background-current term (I_b) added to it. The coefficient δ has no physical meaning but describes how steep the polarographic wave is. In *Eqn. 8*, I_d, I_b, and I_{obs} stand for the limiting diffusion, background, and observed total current; n stands for the number of electrons (*e.g.*, for Pb^{II}, $n=2$), E_{appl} is the stepwise applied potential (in V) at which the total current I_{obs} was recorded, $E_{1/2}$ is the half-wave potential and δ is the reversibility index; F, R, and T have their usual meaning. The parameter δ should be equal to 1 for fully reversible systems. For all practical purposes, δ values above 0.9 indicate reversible systems, and δ values below 0.9 indicate nonreversibility. Typically, δ values between 0.5–0.9 and below 0.5 suggest quasi-reversible and fully irreversible electrochemical reactions, respectively, as defined by *Delahey* [24].

$$I_{obs} = \frac{I_d}{\exp\frac{\delta nF}{RT}(E_{appl} - E_{1/2}) + 1} + I_b \qquad (8)^{2})$$

For the analysis of quasi-reversible DC polarograms with $\delta > 0.8$, the curve-fitting method based on *Eqn. 8*[2]) has been shown to be useful [1]. In the case of a significant decrease in electrochemical reversibility, we have now derived another nonlinear curve-fitting method. This method was essentially developed from an equation for a DC polarographic wave (*Eqn. 9*) derived by *Ružić et al.* [25]. In *Eqn. 9*, I_{red} is the reduction current, I_d the limiting diffusion current, E_{appl} the stepwise applied potential at which the total polarographic current was recorded, α the cathodic transfer coefficient, and $E^{r}_{1/2}$ and $E^{irr}_{1/2}$ the estimated reversible and irreversible half-wave potential, respectively. Note that $E_{1/2}$, the experimental half-wave potential at which a curve was recorded, is not established when *Eqn. 9* is employed. *Ružić et al.* determined $E^{r}_{1/2}$, $E^{irr}_{1/2}$, and α by a graphical logarithmic analysis derived from *Eqn. 9*; this required prior determination of I_d and subtraction of the background current from the polarograms by independent methods. The logarithmic analysis of waves is a tedious process

---

[2]) For the curve fitting of DC polarograms recorded at 25°, as in the original publications, *Eqn. 8* can be implemented as:

$$I_{obs} = \frac{I_d}{10^{\frac{\delta nF}{2.303RT}(E_{appl} - E_{1/2})} + 1} + I_b = \frac{I_d}{10^{((\delta n(E_{appl} - E_{1/2}))/0.05916)} + 1} + I_b$$

The constant $F/2.303RT = 1/0.05916$ V at 25°.

and might not provide accurate enough estimates of reversible half-wave potentials required for the rigorous refinement operations employed in the study of metal/ligand equilibria.

$$\log\left(\frac{I_{red}}{I_d - I_{red}}\right) = \log\left(\exp\frac{nF}{RT}\left(E_{appl} - E^r_{1/2}\right) + \exp\frac{\alpha nF}{RT}\left(E_{appl} - E^{irr}_{1/2}\right)\right) \quad (9)$$

Rearranging *Eqn. 9* to express the reduction current I_{red} as an explicit function of E_{appl} gives *Eqn. 10*. For the direct analysis of a recorded DC polarogram, an appropriate background-current term was added to *Eqn. 10* to obtain the required regression equation (*Eqn. 11*). Parameters that are varied, in a nonlinear curve-fitting operation employing *Eqn. 11*, are I_d, α, $E^r_{1/2}$, $E^{irr}_{1/2}$, and parameters a, b, and c of the background-current term I_b.

$$I_{red} = \frac{I_d}{\exp\frac{nF}{RT}\left(E_{appl} - E^r_{1/2}\right) + \exp\frac{\alpha nF}{RT}\left(E_{appl} - E^{irr}_{1/2}\right) + 1} \quad (10)$$

$$I_{obs} = \frac{I_d}{\exp\frac{nF}{RT}\left(E_{appl} - E^r_{1/2}\right) + \exp\frac{\alpha nF}{RT}\left(E_{appl} - E^{irr}_{1/2}\right) + 1} + I_b \quad (11)$$

Essentially a two-step approach was adopted for the analysis of the recorded DC polarograms. Firstly, *Eqn. 8* was employed to fit the polarograms, thus ascertaining any variation in electrochemical reversibility by monitoring the reversibility index parameter δ. Then, in the case of δ dropping below 0.9, *Eqn. 11* was used to fit the DC polarographic curves which furnished the parameters I_d and $E^r_{1/2}$ for the subsequent use in modelling of the metal/ligand/OH^- systems and refinement of stability constants by *Eqn. 1*.

Results and Discussion. – *Pb^{II}/Glycine/OH^- System*. The main reason given by IUPAC [22] for the wide spread of the reported data for the Pb^{II}/glycine/OH^- system is the fact that Pb^{II} is a hydrolysis-prone metal ion which makes the study of this system difficult, particularly by glass-electrode potentiometry (GEP) (low $[L_T]/[M_T]$ ratios and large $[M_T]$, leading to a narrow pH window for the collection of experimental data before precipitation takes place). *Smith* and *Martell* [21], on the other hand, report a $\log K_1 = 4.6 \pm 0.2$ for the ML complex (value with a large uncertainty). Potentiometry by means of a lead-amalgam electrode made it possible to lower $[M_T]$ and to collect data up to a pH of *ca.* 8 [26][27]; the $\log K_1$ value reported was *ca.* 4.8 ± 0.1. Clearly, even though glycine is a simple and small ligand that is among the most frequently reported ligands in the literature, the speciation of glycine with metal ions such as Pb^{II} makes it rather difficult to study.

This system was now explored by DCP at several fixed $[L_T]/[M_T]$ ratios and variable pH, at 25°, and at an ionic strength of 0.5M (Na,H)NO_3 as a case study, taking advantage *i*) of polarography as a powerful and useful analytical technique for the analysis of metal/ligand systems at low $[M_T]$ and high $[L_T]/[M_T]$ ratios, *ii*) of recent methodologies developed, for the treatment of polarographic data in modelling and computation of

stability constants, and *iii*) of automated instrumentation developed in our laboratories. Also, we checked the applicability of the here proposed nonlinear curve-fitting methods for the analysis of DCP curves.

From *Eqn. 8* it was found that the parameter δ varied between 1 and 0.92 in the entire pH range for which data were recorded (*Fig. 1*). Thus one could regard the recorded polarograms as reversible. It was important now to verify whether the *Ružić*-based equation which was derived for the interpretation of quasi-reversible polarograms could also be implemented for fully reversible curves. *Fig. 1*, *a*, shows that the set of $E^{r}_{1/2}$ values (+) obtained by this method (*Eqn. 11*) was essentially identical to the set of observed $E_{1/2}$ values (○) obtained by *Eqn.* 8. This observation established that, even though *Eqn. 11* might be used for such reversible systems, the initial implementation of the *Eqn. 8* was sufficient. The use of *Eqn. 8* provided, besides information on the electrochemical reversibility as a necessary first step in the interpretation of recorded polarograms, accurate estimates of the observed $E_{1/2}$ (which were essentially the same as $E^{r}_{1/2}$) and I_d values. These two parameters were obtained in a single nonlinear curve-fitting operation. Without loss of generality, the set of I_d and $E_{1/2}$ values (strictly speaking $E^{r}_{1/2}$ values) obtained from the curve-fitting method based on *Eqn. 8* was used in modelling and subsequent refinement operations.

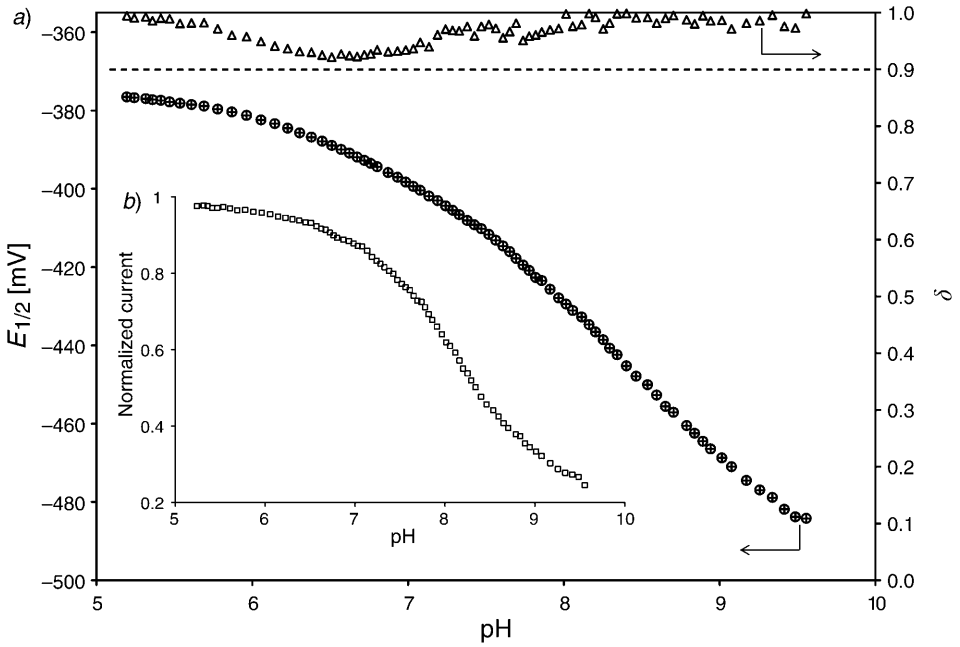

Fig. 1. a) *Comparison of the observed* $E_{1/2}$ (○) *obtained with* Eqn. 8 *and* $E^{r}_{1/2}$ (+) *obtained by the* Ružić*-based curve-fitting method* (*Eqn. 11*)*, both potentials plotted* vs. *pH, for the electrochemically fully reversible* Pb^{II}*/glycine/*OH^- *system for which the reversibility index parameter* δ (△)*, plotted* vs. *pH varied between 1 and 0.9* ($[L_T]/[M_T]=800$, initial $[M_T]=8\cdot10^{-5}$ M, ionic strength 0.5M $(Na,H)NO_3$, *T* 298 K). b) *Variation in normalized limiting diffusion current as a function of pH for the* Pb^{II}*/glycine/*OH^- *system studied by sampled-DC polarography* (experimental conditions as in *a*).

Modelling of the polarographic data was carried out as described previously [6–8][15][20]. A plot of variation in I_d *vs.* pH is shown in *Fig. 1,b*. It is clearly seen that the limiting current has decreased to 0.95 immediately after addition of the ligand. The decrease in I_d and its 'constancy' in the pH range 5 to 6 is in strong support of the formation of the complex $M(HL)^1$). This observation has also been noted in a polarographic study of Cd^{II}/glycine/OH^- where formation of the species M(HL) was found [28]. Between pH 6 and 7.2, there is a small decrease in I_d suggesting formation of a new labile complex.

The significant decrease (down to 0.3) in the limiting diffusion current (most likely due to formation of an inert complex) necessitated the use of virtual potentials [20] for further modelling. The use of reversible half-wave potentials in analysis of slopes is only applicable for fully labile metal/ligand systems [20] when no significant decrease in limiting current takes place. In *Fig. 2*, variation in the observed $E_{1/2}$ and $E_{1/2}$(virt) *vs.* log [L] is shown. Clearly defined slopes (trend lines labelled *A*, *B*, and *C*) corresponding to the formation of ML, ML_2, and ML_3[1]) were obtained with $E_{1/2}$(virt) rather than with the observed $E_{1/2}$; the latter potentials support the formation of only ML and ML_2 (a maximum slope of 60 mV per log unit was observed, see trend line *D* in *Fig. 2*).

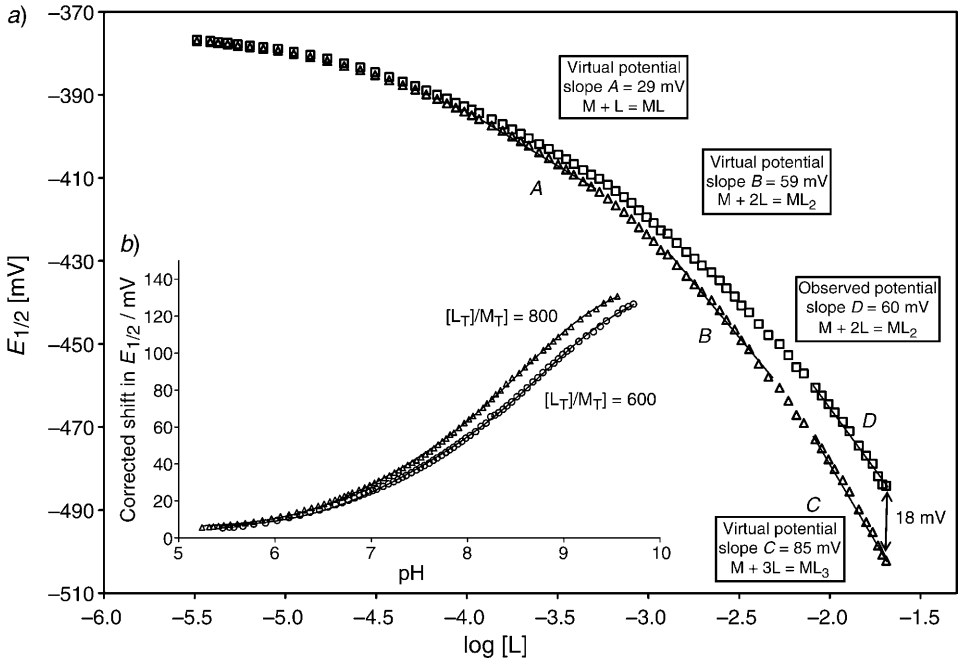

Fig. 2. a) *Variation of virtual* (△) *and observed* (□) *half-wave potential* vs. *log [L] used in the modelling of the* Pb^{II}*/glycine/*OH^- *system studied by DCP* ($[L_T]/[M_T]=800$, initial $[M_T]=8.05\cdot10^{-5}$ M, ionic strength 0.5M (Na,H)NO_3, *T* 298 K; virtual potential from *Eqn. 7*, solid lines indicate trend lines used in the modelling of a metal/ligand/OH^- system, see text for details). b) C*omplex-formation curves computed for the* Pb^{II}*/glycine/*OH^- *system studied by DCP at various* $[L_T]/[M_T]$ *ratios* (points and solid lines indicate the exper. and computed complex-formation curves; stability constants for the final M/L/OH^- model (see *Table 2*) were used to generate the CCFC)

The analysis of $E_{1/2}$(virt) *vs.* pH (not shown) also supported the formation of M(HL), ML, and ML_2. In addition, it prompted the consideration of hydroxo species of the form $ML_q(OH)_r$ in the refinement operations. Above pH 9, the free ligand L^- is a major form of the ligand in solution, and hence a decrease in the slope is expected when complexes such as ML_q are formed. Because of that, the analysis of $E_{1/2}$(virt) *vs.* pH neither provided a direct support for ML_3 formation (identified by the analysis of $E_{1/2}$(virt) *vs.* log L) nor rejected it.

Optimization of a Metal/Ligand Model and Refinement of Stability Constants. The modelling procedure provided the following initial model: M(HL), ML, ML_2, ML_3, ML(OH), $ML(OH)_2$, $ML_2(OH)^{1}$), plus all known Pb^{II} complexes with OH^-. The known stability constants for Pb^{II} complexes with OH^- were compiled from [21] (*Table 1*) and kept fixed during the refinement procedures. This initial model was subjected to further optimization by using the software 3D–CFC. The polarographic complex-formation curves (ECFC as points and CCFC as solid lines) corresponding to the refined stability constants for the identified most plausible model are shown in *Fig. 2*, *b*.

Table 1. *Protonation Constants of the Ligand Glycine* [21], *p*K_w *for Water* [21], *and Formation Constants for* Pb^{II} *Complexes with* OH^- [21] *Included in the* $Pb^{II}/L/OH^-$ *Model and Used in the Refinement of Stability Constants*

Equilibrium	log β	Equilibrium[1])	log β
$H^+ + OH^- \rightleftharpoons H_2O$	13.74	$Pb^{2+} + OH^- \rightleftharpoons Pb(OH)^+$	6.0
$H^+ + L^- \rightleftharpoons HL$	9.54	$Pb^{2+} + 2OH^- \rightleftharpoons Pb(OH)_2$	10.3
$HL + H^+ \rightleftharpoons H_2L^+$	2.39	$Pb^{2+} + 3OH^- \rightleftharpoons Pb(OH)_3^-$	13.3
		$2Pb^{2+} + OH^- \rightleftharpoons Pb_2(OH)^{3+}$	7.6
		$3Pb^{2+} + 4OH^- \rightleftharpoons Pb_3(OH)_4^{4+}$	31.7
		$4Pb^{2+} + 4OH^- \rightleftharpoons Pb_4(OH)_4^{4+}$	35.2
		$6Pb^{2+} + 8OH^- \rightleftharpoons Pb_6(OH)_8^{4+}$	67.4

Table 2 shows the results from the optimization and refinement operations performed with two sets of titration data, *i.e.*, for the ratios $[L_T]/[M_T]$ 600 and 800. The high $[L_T]/[M_T]$ ratios (and low $[M_T]$) were employed to avoid early hydrolysis and precipitation so as to obtain a wide pH range for the collection of the experimental data. A number of models could be refined by the software 3D–CFC, and a systematic way to reach the most plausible model was to generate species-distribution diagrams for the optimized models as well as to check that the models were consistent with the slopes shown in *Fig. 2*. Species-distribution diagrams showed that the formation of the hydroxo species, if they were formed at all, was negligible in the pH range in which the polarographic experiments were performed. For instance, the complex $ML_2(OH)^{1}$) reached 5.7% of the total metal-ion concentration at pH 9.56, the highest pH at which the experiment was terminated, for the $[L_T]/[M_T]$ ratio of 800. Because of that, the refined stability constants for this hydroxo species had high uncertainty (large standard deviations). It should be noted that the species ML_3 has not been reported in the literature. Inclusion of one of the hydroxo species in the model in place of ML_3 led to higher values of the overall fit (*Eqn. 2*) than with the models that included ML_3. Since the graphical modelling in *Fig. 2*, *a*, strongly suggested the existence of the species ML_3,

it was plausible to include it in the optimization procedures. It was gratifying to observe that there was no significant effect on the computed stability constants for the complexes M(HL) and ML, regardless of the inclusion or exclusion of the hydroxo species $ML_q(OH)_r$; the computed stability constant for ML_2 was slightly lower when ML(OH) was included with both stability constants having large standard deviation. These results suggested that the most plausible optimized model is the one without any metal-ligand hydroxo species (see *Fig. 3,a*). The computed stability constants found here for the complexes M(HL) and ML are, in principle, identical to those reported by *Smith* and *Martell* [21]. However, our stability constant for ML_2 is slightly lower. This is not surprising since the complex ML_3 has not been reported when other experimental techniques were used.

Table 2. *Overall Stability Constants for Pb^{II} with Glycine Found by DCP at 25° and an Ionic Strength (μ) of 0.5 M in $NaNO_3$ and Those Reported Elsewhere*

$[L_T]/[M_T]$	$[M_T]$/M	log β^1)						*OF*/mV[a])	Ref.
		M(HL)	ML	ML_2	ML_3	ML(OH)	$ML_2(OH)$		
600	$8.06 \cdot 10^{-5}$	10.56 ± 0.04	4.56 ± 0.01	7.09 ± 0.02	9.25 ± 0.02	excluded	excluded	0.360	this work
		10.56 ± 0.04	4.56 ± 0.01	6.97 ± 0.05	9.0 ± 0.1	9.7 ± 0.1	excluded	0.347	this work
800	$8.05 \cdot 10^{-5}$	10.45 ± 0.04	4.59 ± 0.01	7.28 ± 0.03	9.29 ± 0.03	excluded	excluded	0.345	this work
		10.46 ± 0.04	4.58 ± 0.01	7.29 ± 0.04	9.25 ± 0.09	excluded	10.9 ± 0.8	0.342	this work
Final model[b])		10.51 ± 0.06	4.58 ± 0.02	7.19 ± 0.10	9.27 ± 0.02	excluded	excluded	–	this work
Literature data		10.56[c])	4.6 ± 0.2[d])	7.5 ± 0.1[d])	not reported	10.7[e])	not reported	–	[21]
		11.1 ± 0.1[d])	4.76 ± 0.07[d])	7.4 ± 0.1[d])	not reported	not reported	not reported	–	[27]

[a]) *OF* (= Overall fit) is a statistical parameter for voltammetric data and stands for the overall fit of the CCFC to the ECFC. [b]) Final model: averaged values from data for ratios 600 and 800 for the models containing M(HL), ML, ML_2, and ML_3[1]). [c]) μ = 1.0 M, 25°, Pb(Hg) ISE (ion specific electrode), potentiometry. [d]) μ = 0.5 M, 25°. [e]) μ = 3.0 M, 25°, high uncertainty.

The presence of the species $M(HL)_2$ and $M(HL)_3$ has been proposed in [21], but the formation of these species was considered implausible and not included in our model. A species distribution diagram (see *Fig. 3,b*) generated for the total metal-ion and total ligand concentrations used in our study but with the stability constants from the literature model showed that the species $M(HL)_2$ and $M(HL)_3$ formed at pH values lower than 6 and their formation would not be detectable; they form under M(HL) and exist in solution to a maximum fraction of *ca.* 3% at a pH of *ca.* 4.5. This literature model also suggested that the species ML_2 would be predominant above pH 8. This should have led to the observation of a constant slope of *ca.* 60 mV per log unit in the plot of $E_{1/2}$(virt) *vs.* log [L] (see *Fig. 2,a*), instead a slope of *ca.* 85 mV per log unit was observed. The virtual potentials generated from the polarographic data,

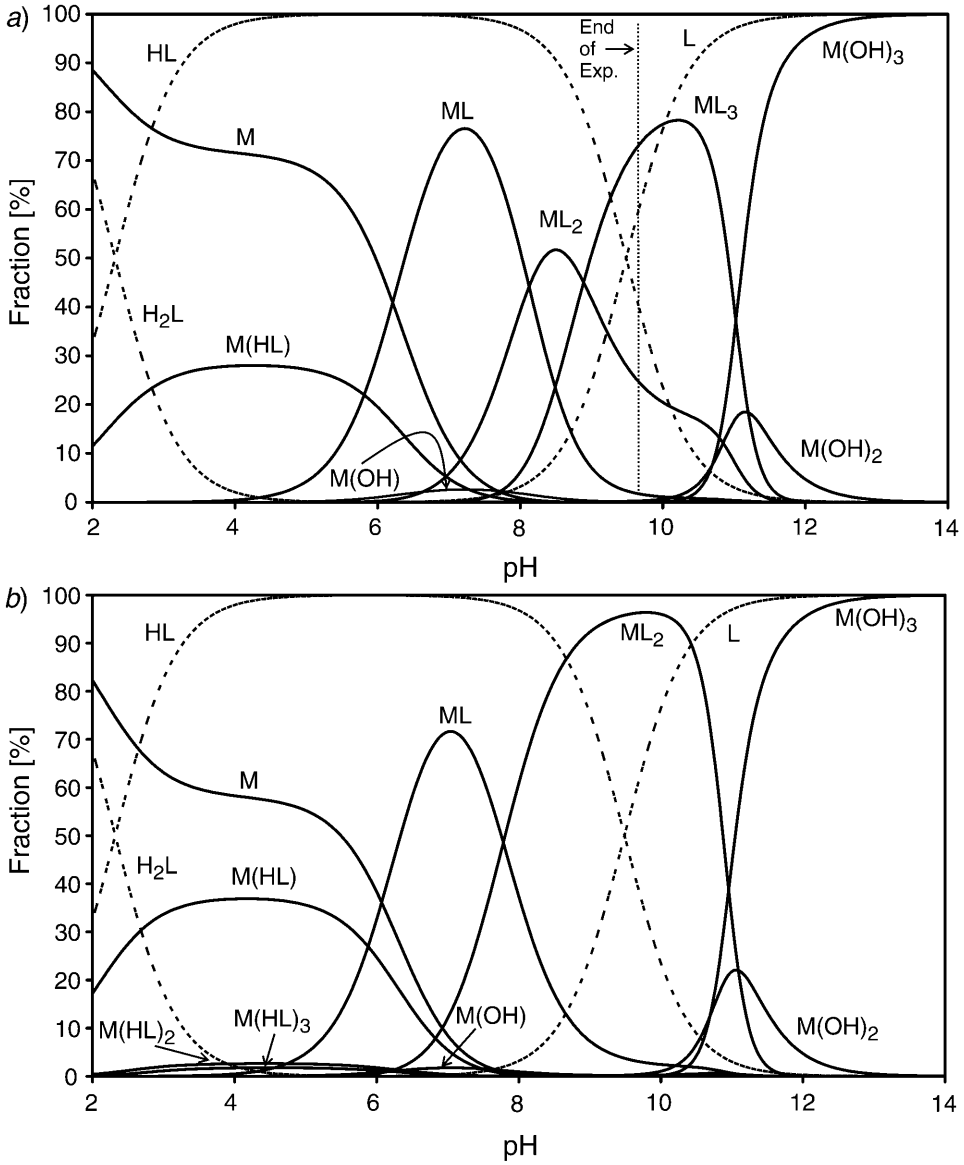

Fig. 3. *Species distribution*[1]) *for a* Pb^{II}*/glycine/OH system as a function of pH computed for the used experimental conditions* ($[L_T]/[M_T]=800$ *and* $[M_T]=8.05\cdot10^{-5}$ M*;* all known stability constants for the $Pb_x(OH)_y$ complexes [21] were included): a) *stability constants for the final M/L/OH model with M(HL), ML,* ML_2*, and* ML_3 *from* Table 2*;* b) *stability constants from* [21] *for the model with M(HL),* $M(HL)_2$*,* $M(HL)_3$*, ML, and* ML_2. The dotted vertical line indicates the pH at which the experiment was terminated (just prior the predicted precipitation).

together with the appropriate experimental conditions, were entered into the program ESTA [29–31], and the stability constants for the proposed model were refined. Difficulties in refinement were encountered by the program ESTA if all the stability constants for the proposed model were allowed to be refined. It should be realized, however, that the experimental conditions employed ($[L_T]/[M_T]$ ratios >400) were not typical for potentiometry. The high $[L_T]/[M_T]$ ratios employed as well as the refinement of the data in the pH region where the ligand becomes fully deprotonated were likely to be the cause of the difficulties experienced in the refinement operations performed by ESTA. However, fixing the stability constants for M(HL) and/or ML, obtained from the refinement of the polarographic data (*Table 2*), and simultaneously refining the initial $[H^+]$ led to a reasonable refinement of the stability constants for the complexes ML_2 and ML_3; ESTA accepted the formation of ML_3. This observation suggests that the most successful application of virtual potentiometry in the refinement of virtual potentiometric data by a dedicated potentiometric software is to be expected when relatively low $[L_T]/[M_T]$ ratios are used in the polarographic studies.

Pb^{II}/Sarcosine/OH^- System. To the best of our knowledge, there are no data reported in the literature on the formation of complexes between Pb^{II} and sarcosine. The only reasonable explanation for this might be a supposition that lead complexes with sarcosine are weaker than those with glycine, and any attempt of studying the system by GEP failed.

In general, the protocol implemented for the Pb^{II}/glycine/OH^- system was employed also here. However, the system Pb^{II}/sarcosine/OH^- showed a significant departure from electrochemical reversibility, characteristics not observed for the Pb^{II}/glycine/OH^- system. The parameter δ varied from 0.93 to *ca.* 0.65 at the highest pH of 9.65 at which the experiment was terminated (*Fig. 4*). It became obvious that for any rigorous data evaluation, the curve-fitting operation based on *Eqn. 11* had to be performed. It is seen in *Fig. 4* that the difference between the experimentally observed $E_{1/2}$ and $E^r_{1/2}$ reached a value of 9 mV. In all following modelling and refinement operations, the reversible potentials were employed. The values for fitted parameters (from *Eqn. 11*) seen in *Fig. 4* are reported with standard deviations to indicate the goodness-of-fit achieved.

The analyses of the normalized limiting diffusion current showed a decrease to a value of 0.64; this is not a decrease as large as that observed for the system involving glycine but nevertheless significant enough to require the use of the virtual potential in modelling operations. Analysis of variations in $E_{1/2}$(virt) *vs.* pH (*Fig. 5,a*) and *vs.* log [L] (*Fig. 5,b*) resulted in M(HL), ML, ML_2, ML_3, and $ML_p(OH)_r$[1]) complexes that were identified by the protocols described above. The continuous variation of the virtual potential observed in *Fig. 5*, particularly in *Fig. 5,b*, indicates that the complexes ML, ML_2, and ML_3 are formed in consecutive fashion and that there is a large overlap in the pH and log [L] regions where they exist simultaneously. Also, it appears that complex ML_3 does not form to a large extent as there is not a well-defined log [L] region with a slope of *ca.* 90 mV as expected for this complex. From this follows that the slope marked by the solid line *C* in *Fig. 5,a* must be attributed mainly to the formation of a significant amount of $ML_q(OH)_r$ complexes. Here again, a careful analysis of the complex-formation curves combined with the species-distribution diagrams was performed. Examples of refined models for the $[L_T]/[M_T]$ ratio 400 are shown in *Table 3*.

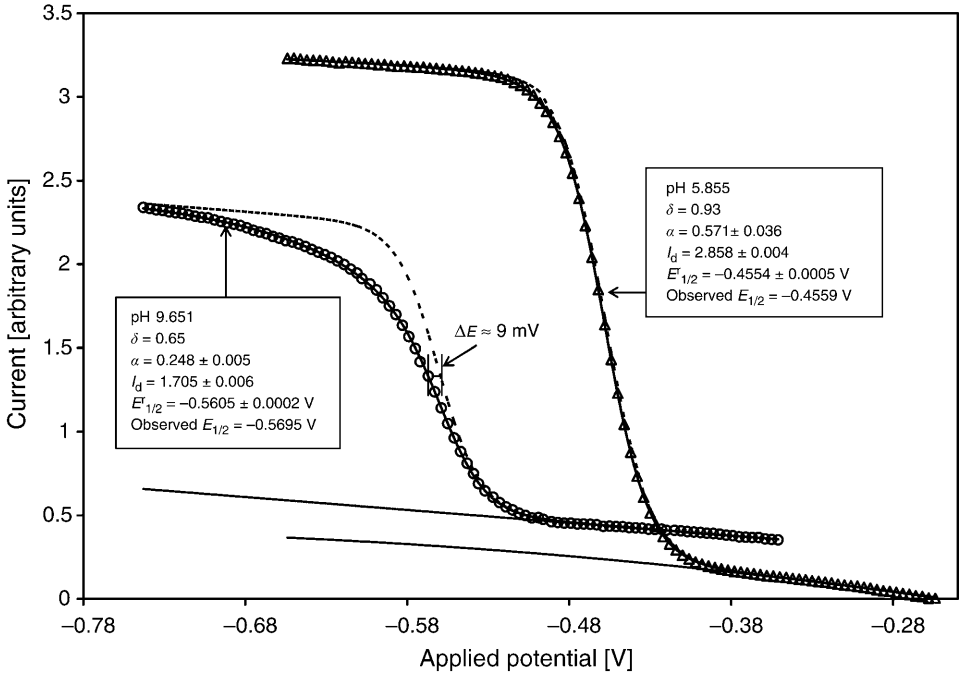

Fig. 4. *Examples of analyses of DC polarograms from the study of the Pb^{II}/sarcosine/OH^- system.* $[L_T]/[M_T] = 400$, $[M_T] = 7.99 \cdot 10^{-5}$ M, ionic strength 0.5M (Na,H)NO_3, *T* 298 K. Experimental points (△ and ○) represent the recorded current at a particular applied potential; solid and dotted lines represent experimental and fully reversible, resp., polarograms computed with parameters obtained from the *Ružić*-based curve-fitting method (*Eqn. 11*). Parameter δ is from *Eqn. 8*.

An attempt to exclude OH-containing species failed; one can see a poor *OF* generated by optimization and refinement operations. A good *OF* was obtained with inclusion of either $ML_2(OH)$ and/or $ML_2(OH)_2$; both these complexes had no significant impact on refined stability constants of M(HL), ML, and ML_2. Species-distribution diagrams suggested that if the complex $ML_2(OH)$ was formed then it would constitute a very small fraction of the total metal-ion concentration. The standard deviation for this complex is large when compared with the one obtained for the complex $ML_2(OH)_2$ (see *Table 3*).

Analysis of the data in *Table 3* reveal that the final model proposed for the Pb^{II}/sarcosine/OH^- system consists of M(HL), ML, ML_2, ML_3, and $ML_2(OH)_2$[1]) for which stability constants, as $\log \beta$, were determined to be 11.01 ± 0.04, 4.18 ± 0.03, 7.23 ± 0.06, 9.1 ± 0.3, and 15.97 ± 0.07, respectively. The solid line seen in *Fig. 6,a* represents the computed complex-formation curve for the final Pb^{II}/sarcosine/OH^- model. For any practical reasons, the CCFC can be regarded as reproducing the experimental curve (○) very well. The species-distribution diagram computed for the final M/L/OH^- model under experimental conditions for the $[L_T]/[M_T]$ ratio 400 (see *Fig. 6,b*) confirms all the above considerations. Indeed, in the pH range between 7 and 9, all the five metal complexes with the ligand sarcosine are formed simultaneously. It is also seen that Pb(OH) is formed to a significant degree. The complex ML_3 might be regarded as a

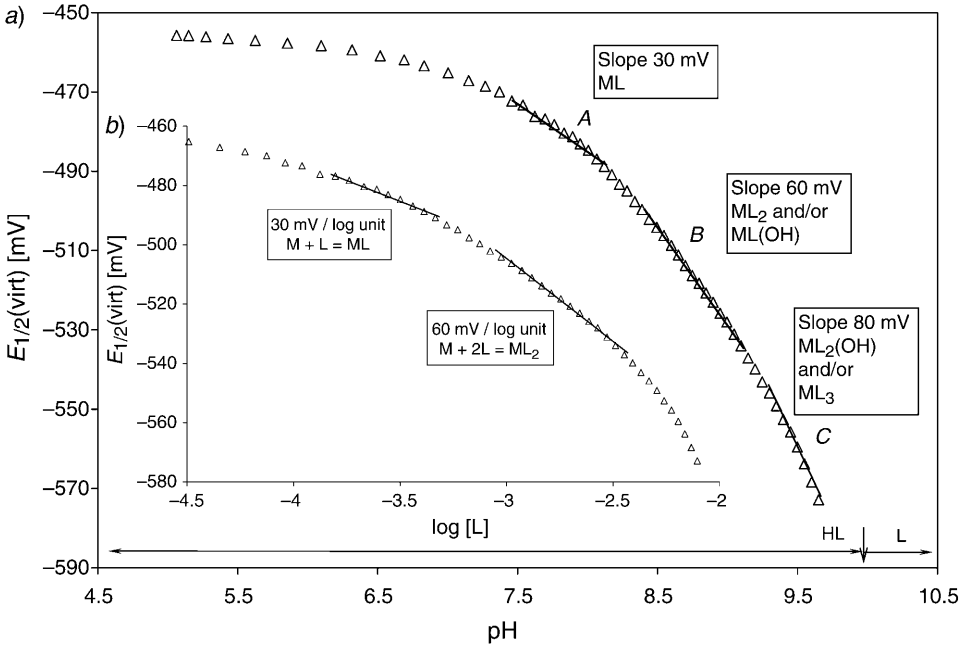

Fig. 5. *Prediction of major metal-containing species for the Pb^{II}/sarcosine/OH^- system from the analysis of variation in* $E_{1/2}$(*virt*) *as a function of* a) *pH and* b) *log [L]*. $[L_T]/[M_T] = 400$, ionic strength 0.5M (Na,H)NO_3, 25°, initial $[M_T] = 7.99 \cdot 10^{-5}$ M; solid lines indicate trend lines used in modelling operations, see text for details.

Table 3. *Overall Stability Constants for Pb^{II} with Sarcosine by DCP at* 25° *and an Ionic Strength of 0.5*M *in $NaNO_3$.* $[L_T]/[M_T] = 400$, initial $[M_T] = 7.99 \cdot 10^{-5}$ M.

Type of $E_{1/2}$ used	$\log \beta^1$)						*OF*/mV[a])	Remarks
	M(HL)	ML	ML_2	ML_3	$ML_2(OH)$	$ML_2(OH)_2$		
Reversible $E^r_{1/2}$	10.95 ± 0.05	4.28 ± 0.02	6.48 ± 0.24	9.89 ± 0.02	excluded	excluded	1.508	poor fit
	excluded	4.18 ± 0.03	6.09 ± 0.46	9.81 ± 0.02	excluded	excluded	1.6256	poor fit
	11.00 ± 0.04	4.19 ± 0.03	7.20 ± 0.06	9.11 ± 0.32	excluded	15.98 ± 0.06	0.437	plausible model
	11.01 ± 0.04	4.19 ± 0.03	7.22 ± 0.06	excluded	11.23 ± 0.36	15.95 ± 0.09	0.444	plausible model
	11.02 ± 0.04	4.17 ± 0.02	7.28 ± 0.02	excluded	excluded	16.06 ± 0.02	0.471	plausible model
Observed $E_{1/2}$	11.10 ± 0.04	4.63 ± 0.02	5.86 ± 2.22	9.91 ± 0.08	excluded	16.27 ± 0.06	1.424	poor fit
Final model[b])	11.01 ± 0.04	4.18 ± 0.03	7.23 ± 0.06	9.1 ± 0.3	–	15.97 ± 0.07		

[a]) *OF* (= Overall fit) is a statistical parameter for voltammetric data and stands for the overall fit of the CCFC to the ECFC. [b]) Stability constants derived from most plausible refined models.

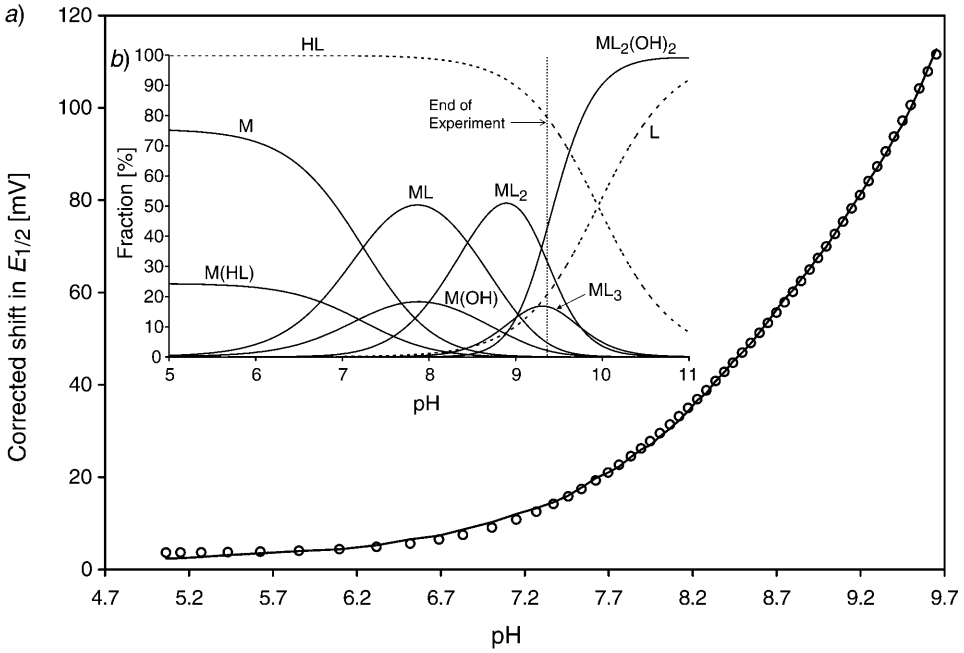

Fig. 6. *Optimization of the Pb^{II}/sarcosine/OH^- model and refinement of stability constants based on the DCP data obtained from acid–base titration:* a) *experimental* (○) *and computed* (solid line) *complex-formation curves.* b) *Species-distribution*[1]) *diagram as a function of pH.* $[L_T]/[M_T]=400$, ionic strength 0.5M (Na,H)NO_3, 25°, $[M_T]=7.99\cdot10^{-5}$ M. Stability constants for the final model consisting of M(HL), ML, ML_2, ML_3, and $ML_2(OH)_2$ are from *Table 3*. The dotted vertical line indicates the pH at which the experiment was terminated (just prior the predicted precipitation).

minor species when compared with ML, ML_2, and $ML_2(OH)_2$, and hence no well-defined slope for this complex is observed in *Fig. 5*, *b*.

In all the above operations, the theoretically predicted rather than observed half-wave potential was used. The difference between the two was rather small and reached a maximum value of *ca.* 9 mV. It was important to test whether the predicted difference had any significant influence on the refined stability constants; results obtained are shown in *Table 3*. The differences between the stability constants generated from reversible and observed potentials can be considered as rather large; in the case of ML_2, the stability constant decreased by over one log unit and had a large standard deviation. From the literature data [21] it follows that stability constants for Cu^{2+}, Zn^{2+}, and Ni^{2+} with the ligand glycine are somewhat larger (a fraction of a log unit) when compared with corresponding metal complexes with the ligand sarcosine. The same trend was obtained for Pb^{II} with log K_1 of 4.58 and 4.18 for glycine and sarcosine, respectively. Since the observed potential generated a slightly larger log K_1 for sarcosine than for glycine, one might conclude that the observed potential must not be used when a departure from electrochemical reversibility takes place, even though it appears to be a small one. All the above results strongly support the theories and mathematical procedures implemented in this work. DCP supported by the protocol and equipment described

above proved to be a powerful and reliable analytical technique for the study of metal complexes of samples showing involved heterogeneous kinetics (quasi-reversible electrochemical reduction process) as well as involved homogeneous kinetics, *i.e.*, when labile and inert metal complexes are formed simultaneously. An additional advantage of DCP was also convincingly demonstrated here, namely the ability to work at large total ligand-to-metal-ion concentration ratios $[L_T]/[M_T]$ and small total metal-ion concentration $[M_T]$ that resulted in the formation of metal complexes involving the ligand of interest with simultaneous suppression of hydrolysis of the metal ions; the experimental conditions employed allowed for a large pH window suitable for the study of metal complexes.

The authors thank the University of Pretoria and the *National Research Foundation* for their generous financial support.

Experimental Part

Materials. The ligands glycine (M_r 75.07; 99% pure) and sarcosine (M_r 89.09; 99% pure) were purchased from *Aldrich* (Milwaukee, USA). All ligands were used as received, in their solid form as free acids. Cadmium nitrate tetrahydrate ($Cd(NO_3)_2 \cdot 4\,H_2O$; M_r 308.47; 99% pure) and lead nitrate ($Pb(NO_3)_2$; M_r 331.20; 99% pure) were of anal. grade from *Aldrich*. All other reagents used were of anal. grade from *Saarchem* (Muldersdrift, South Africa). Deionized H_2O was obtained by passing dist. H_2O through a *Milli-Q*-water-purification system (*Millipore*, Bedford, MA, USA). The 0.05M stock solns. of cadmium and lead nitrates were prepared in deionized H_2O and adjusted to an ionic strength of 0.5M with $NaNO_3$. A standard HNO_3 soln. was prepared by dilution of concentrated acid and titration with the primary standard disodium tetraborate (borax). The concentration of a standard NaOH soln. was established by titration with potassium hydrogen phthalate (KHP). The base and acid solns. were adjusted to an ionic strength of 0.5M by addition of $NaNO_3$.

Instrumentation. All experiments were performed in a *Metrohm* water-jacketed glass vessel, equipped with a model *728* magnetic stirrer (*Metrohm*) and thermostatted at $25.0 \pm 0.1°$ by circulating water from a constant-temp. bath. For GEP and DCP experiments, a dedicated computer-controlled instrumental set-up was developed in our laboratories. Several commercial stand-alone instruments and hardware built in-house were interfaced to a personal computer (PC), equipped with dedicated virtual-instrument software modules for automated data acquisition. A block diagram of the automated instrumental setup is shown in *Fig. 7*.

A 1.8-GHz Pentium PC working under Windows XP was used as the workstation for the instrumental setup developed. A LabVIEW software package version 7.0 (*National Instruments*, Austin, Texas, USA) was the platform used to develop the various virtual-instrument (VI) software modules for the acquisition of the GEP and DCP data. LabVIEW is an object-oriented visual programming language based on the dataflow programming environment designed for programming data acquisition, data handling, and data display.

The data acquisition (DAQ) card used to interface the instrumental setup to the PC was a *NI-6036-E* low-cost multifunction input/output card (*National Instruments*) featuring 16 single-ended or 8 differential, gain-programmable analog input channels with a guaranteed sampling rate of 200 kHz. The analog input channels are multiplexed to a 16-bit analog-to-digital converter (ADC). Furthermore, the DAQ card has two analog output channels based on two 16-bit digital-to-analog converters (DACs). The analog input/output range can be programmed to the maximum bipolar input/output range of ± 10 V. In addition, the DAQ card has 8 digital I/O lines and two 24-bit counter/timer channels for high-precision, time-critical measurements (base clock frequency of 20 MHz). The DAQ card was connected to the hardware components by means of *SCB-68* shielded connector block from *National Instruments*.

For potentiometric and temperature measurements of a sample, either a *713* or *780* pH meter (both from *Metrohm*) was used. The pH meters worked at sensitivities of ± 0.1 mV (± 0.001 pH). A *Metrohm*-

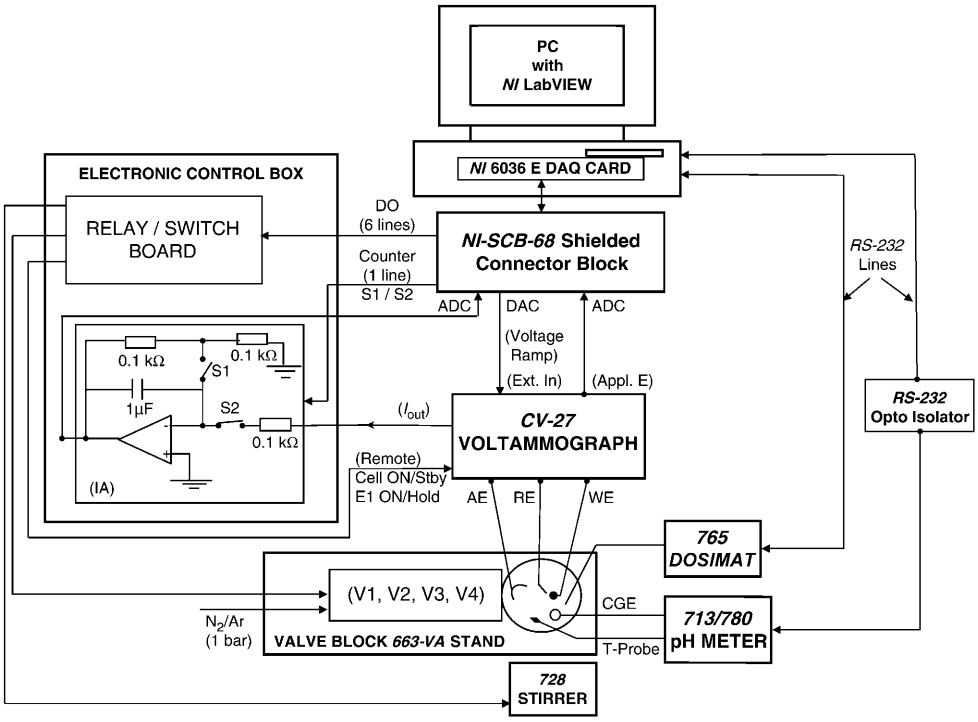

Fig. 7. *Block diagram showing interfacing and connectivity of the various hardware components of the instrumental setup developed for potentiometric and polarographic measurements.* CGE = Combination glass electrode; AE = auxiliary electrode; RE = reference electrode; WE = working electrode; T-Probe = temperature probe; ADC = analog-to-digital converter; DAC = digital-to-analog converter; DO = digital output; IA = integration amplifier; V1, V2, V3, and V4 are solenoid valves on the valve block of the *663-VA* stand. For more details, see text.

6.0234.100 combination glass electrode (CGE) was used for potentiometric measurements. Temp. measurements were performed with a *Pt-1000* temp. probe (T-Probe) from *Metrohm* (model *6.1110.100*). Automatic additions of reagents were achieved with a digital *Metrohm-765-Dosimat* burette. The pH meter and the digital burette were connected to the PC through serial ports and were controlled by *RS-232* protocols implemented in the software modules. To prevent electronic interferences due to ground potential differences of the pH meter and the rest of the instrumental setup, a *DLP-510-RS-232* opto isolator module (*Clearline*, Midrand, South Africa) was used for optical isolation of the pH meter from the rest of the electronic components.

Polarographic measurements were performed in the valve block of a *Metrohm-663-VA* stand equipped with a multimode electrode (*Metrohm*; model *6.1246.020*) as a working electrode (WE), used in the dropping-mercury electrode mode. *Metrohm* electrodes Ag/AgCl (3M KCl) and Pt rod were used as reference and auxiliary electrodes (RE and AE), resp. High-purity N_2 was used for the deaeration of the sample solns. and for the delivery of 1 ± 0.2 bar pressure required for the operation of the solenoid valves V1, V2, V3, and V4 on the valve block of the *663-VA* stand. Dedicated digital-output (DO) lines of the DAQ card were used to control the appropriate solenoid valves of the *663-VA* stand for the mercury-drop formation and dislodge as well as for the N_2-gas inlet for the deaeration of the soln. The solenoid valves

were operated *via* appropriate relay or digital switches placed in a shielded electronic control box built in-house. A dedicated DO line of the DAQ card was also used for the computer control of the *728* magnetic stirrer.

Potentiostatic control and current measurements to and from the voltammetric cell were achieved with a *CV-27* voltammograph (*Bioanalytical Systems*, Indiana, USA). The *CV-27* voltammograph is provided with an external potential control and signal output to an external recording device, a current-to-voltage converter with gain (2 μA/V to 10 mA/V), among other functionalities. To increase the sensitivity of the current measurements (I_{out}) from the *CV-27* voltammograph and to minimize the noise level, an integration-amplifier (IA) circuitry placed in the in-house built electronic control box was incorporated. The control functions, cell connection (Cell On/Standby) and potentiostatic mode (E1 ON/Hold) of the *CV-27* voltammograph were actuated by a remote timer (*Remote* socket) by using TTL logic signals from dedicated DO lines of the DAQ card.

In the instrumental system of *Fig. 7*, the voltage ramp for sampled-DC polarography was digitally generated. Each potential of the digital waveform was converted to an analog potential *via* one of the DAC channels of the DAQ card. The potential was then applied to the WE through the summing point of the *CV-27* voltammograph. A single counter channel was used for simultaneous digital control of the switches S1 and S2 (*Fig. 7*). The TTL pulses from the counter line were also used to trigger the acquisition of the current and applied potential. In the instrumental system of *Fig. 7*, two DAC channels of the DAQ card, in differential mode, were used for acquisition of integrated cell current and applied potentials from the IA and the *CV-27* voltammograph.

In metal/ligand studies by GEP and DCP, several programs (so called virtual instruments or VIs) were developed for automated experiments. Three main VIs were developed to achieve *i*) recording of a single sampled-current polarogram with the user being in charge of when to record such a polarogram, *ii*) performing an automated data acquisition in a titration of a soln. sample whereby only GEP data are collected, or *iii*) performing an automated titration with acquisition of both GEP and DCP data on a single soln. sample (with GEP being the leading technique to establish soln. equilibration). The virtual instruments allowed monitoring of soln. equilibration. Constancy in the pH readings was monitored in a statistical fashion, by using user-defined parameters for the sampling rate and criterion of stability. Full histories of time taken to establish equilibrium, the CGE-potential readings recorded at each titration step were automatically saved into a data file in a spreadsheet format for subsequent analysis by the user. The current–potential data for each recorded polarogram were saved in different data files generated online in ASCII format for easy transfer for the subsequent analysis of the polarograms. The software modules for automated acquisition of DCP data included, among other functionalities, online adjustment of the potential window for recording polarograms since there is a shift in half-wave potential when complexes are formed in solution. The detailed descriptions of circuitry and flow-chart diagrams of the full functionalities of the instrumental setup developed are available on request from the authors.

Analytical Procedure and calibration of the CGE. The combination glass electrode (CGE) was calibrated by strong acid–strong base titration before and after a polarographic experiment. In a typical calibration experiment, a 10.00-ml aliquot of standardized HNO_3 soln. (adjusted to an ionic strength of 0.5M with $NaNO_3$) was mixed with 20.00 ml of 0.5M $NaNO_3$ background electrolyte in the thermostatted titration vessel and titrated with a standardized soln. of NaOH (also adjusted to an ionic strength of 0.5M). The calibration titrations were performed automatically by means of the dedicated LabVIEW-controlled instrumental setup depicted in *Fig. 7*. The titrant-volume increments were set between 0.1 and 0.2 ml. Readings in the potential of the CGE (E_{CGE}) were typically collected in the pH range 1.0–2.5 and 11.5–12.5. Exper. points E_{CGE} *vs.* pH were fitted with a straight line to establish the value of E° and a response slope of the CGE. The values of E° and a response slope were used to calculate $pH = -\log_{10}[H]$ of a sample under investigation.

Acid-Base Titrations in Polarographic Studies of Metal/Ligand Systems. To 30.0 ml of the background electrolyte (0.5M $NaNO_3$) in the cell, a few corns of solid gelatine were added for the suppression of polarographic maxima. Ultra-high-purity N_2 gas was passed through the soln. for at least 20 min. The purity of the background electrolyte was checked by recording a DC polarogram of this soln. followed by addition of the required volume of the lead(II) standard soln. to achieve the desired initial total

metal-ion concentration [M_T] of *ca.* $8 \cdot 10^{-5}$ M. A polarogram was recorded and repeated twice for the determination of $E_{1/2}$(M) and I_d(M) of Pb^{II} in the absence of the ligand. The ligand glycine or sarcosine was introduced into the titration vessel by accurately transferring an appropriate amount of the solid ligand to achieve the required [L_T]/[M_T] ratio. The dedicated LabVIEW-based virtual instrument was employed to automatically collect the experimental data within a preset pH range. Standardized NaOH soln. (adjusted to an ionic strength of 0.5M) in a 5-ml burette cylinder placed on the digital *765-Dosimat* burette was used to vary the pH. A series of 70–80 polarograms were recorded with the sample solns. at pH increments of 0.05 to 0.10 pH units.

REFERENCES

[1] I. Cukrowski, J. M. Zhang, *Electroanalysis* **2004**, *16*, 612.
[2] J. J. Lingane, *Chem. Rev.* **1941**, *29*, 1.
[3] D. D. DeFord, D. N. Hume, *J. Am. Chem. Soc.* **1951**, *73*, 5321.
[4] D. N. Hume, D. D. DeFord, G. C. B. Cave, *J. Am. Chem. Soc.* **1951**, *73*, 5323.
[5] D. R. Crow, in 'Polarography of Metal Complexes', Academic Press, London, New York, 1969.
[6] I. Cukrowski, J. M. Zhang, A. van Aswegen, *Helv. Chim. Acta* **2004**, *87*, 2135.
[7] I. Cukrowski, J. M. Zhang, *Chem. Anal.* **2005**, *50*, 3.
[8] J. Heyrovský, J. Kůta, in 'Principles of Polarography', Academic Press, London, New York, 1966.
[9] H. Matsuda, Y. Ayabe, *Bull. Chem. Soc. Jpn.* **1955**, *28*, 422.
[10] H. Matsuda, Y. Ayabe, *Bull. Chem. Soc. Jpn.* **1956**, *29*, 132.
[11] H. Matsuda, Y. Ayabe, *Z. Elektrochem.* **1959**, *64*, 1164.
[12] V. Kačena, L. Matoušek, *Chem. List.* **1952**, *46*, 525.
[13] V. Kačena, L. Matoušek, *Collect. Czech. Chem. Commun.* **1953**, *18*, 294.
[14] I. Cukrowski, M. Adsetts, *J. Electroanal. Chem.* **1997**, *429*, 129.
[15] I. Cukrowski, *Electroanalysis* **1997**, *9*, 1167.
[16] I. Cukrowski, S. A. Loader, *Electroanalysis* **1998**, *10*, 877.
[17] I. Cukrowski, R. D. Hancock, R. C. Luckay, *Anal. Chim. Acta* **1996**, *319*, 39.
[18] I. Cukrowski, *Electroanalysis* **1999**, *11*, 606.
[19] I. Cukrowski, *J. Electroanal. Chem.* **1999**, *460*, 197.
[20] I. Cukrowski, D. M. Mogano, J. R. Zeevaart, *J. Inorg. Biochem.* **2005**, *99*, 2308.
[21] R. M. Smith, A. E. Martell, 'NIST Standard Reference Database 46. NIST Critically Selected Stability Constants of Metal Complexes Database', Version 8.0, US Department of Commerce, National Institute of Standards and Technology, 2004.
[22] IUPAC Analytical Chemistry Division, Commission on Equilibrium Data, *Pure Appl. Chem.* **1991**, *63*, 597.
[23] I. Cukrowski, '3D-CFC Program', Windows version 1.2.1, unpublished.
[24] P. Delahey, *J. Am. Chem. Soc.* **1953**, *75*, 1430.
[25] I. Ružić, A. Baric, M. Branica, *J. Electroanal. Chem.* **1971**, *29*, 411.
[26] J. Berggren, O. Börtin, S. Gobom, *Acta Chem. Scand. A* **1988**, *42*, 685.
[27] A. Casale, A. De Robertis, C. De Stefano, A. Gianguzza, G. Patane, C. Rigano, S. Sammartano, *Thermochim. Acta* **1995**, *225*, 109.
[28] I. Cukrowski, G. Ngigi, *Electroanalysis* **2001**, *13*, 1242.
[29] F. Marsicano, C. Monberg, B. S. Martincigh, K. Murray, P. M. May, D. R. Williams, *J. Coord. Chem.* **1998**, *16*, 321.
[30] P. M. May, K. Murray, D. R. Williams, *Talanta* **1988**, *35*, 23.
[31] P. M. May, K. Murray, *Talanta* **1988**, *35*, 927.

Received January 6, 2006